The spalling decay of building bioclastic limestones of Provence (South East of France): From clay minerals swelling to hydric dilation

Jérémie Berthonneau, Philippe Bromblet, Fabien Cherblanc, Eric Ferrage, Jean-Marc Vallet, O. Grauby

▶ **To cite this version:**

Jérémie Berthonneau, Philippe Bromblet, Fabien Cherblanc, Eric Ferrage, Jean-Marc Vallet, et al.. The spalling decay of building bioclastic limestones of Provence (South East of France): From clay minerals swelling to hydric dilation. Journal of Cultural Heritage, 2016, 17, pp.53-60. 10.1016/j.culher.2015.05.004 . hal-01235442

HAL Id: hal-01235442
https://hal.science/hal-01235442

Submitted on 30 Nov 2015

HAL is a multi-disciplinary open access archive for the deposit and dissemination of scientific research documents, whether they are published or not. The documents may come from teaching and research institutions in France or abroad, or from public or private research centers.

L'archive ouverte pluridisciplinaire **HAL**, est destinée au dépôt et à la diffusion de documents scientifiques de niveau recherche, publiés ou non, émanant des établissements d'enseignement et de recherche français ou étrangers, des laboratoires publics ou privés.

The spalling decay of building bioclastic limestones of Provence (South East of France): from clay minerals swelling to hydric dilation

JEREMIE BERTHONNEAU[1*], PHILIPPE BROMBLET[2], FABIEN CHERBLANC[3], ERIC FERRAGE[4], JEAN-MARC VALLET[2] and OLIVIER GRAUBY[1]

[1] Aix Marseille Université, CNRS, CINaM UMR 7325, Campus de Luminy, 13288 Marseille, France.

[2] CICRP Belle de Mai, 21 rue Guibal, 13003 Marseille, France.

[3] LMGC, CNRS, Université Montpellier 2, Place Eugène Bataillon, 34000 Montpellier, France.

[4] IC2MP, CNRS, Université de Poitiers, 40 Avenue du Recteur Pineau, F-86022 Poitiers Cedex, France.

*Corresponding author, e-mail: berthonneau@cinam.univ-mrs.fr

Abstract:

Medieval historical monuments of the Provence region (South East of France) were erected with bioclastic limestones and display different sensitivities to spalling decay. The present study aims at understanding the physical processes at play as well as the internal properties governing its intensity. Limestones of contrasting sensitivity to spalling were compared to a reference type, unaffected by this decay, by means of petrography, petrophysic, mineralogy, and hydro-mechanics. The obtained results highlighted that the various sensitivities can be explained by the deformation recorded during water content variation (hydric dilation). A clay fraction was systematically detected within the mineralogical composition except for the reference material, and some swelling layers were identified in montmorillonite/glauconite mixed layer minerals. A specific quantification procedure based on the combination of transmission electron microscopy coupled to an energy-dispersive X-ray spectrometer (TEM-EDX) and profile modeling of X-ray diffraction patterns was applied. A strong relationship between swelling layer content and hydric dilation of limestones was evidenced and corroborated the spalling sensitivity. Further interpretation of results showed that swelling layers localization within the texture significantly influence hydric dilation kinetics. Eventually, a mechanical softening was measured after water saturation. This behavior seems unrelated to the clay mineral content and its relative influence on spalling should be examined.

Keywords:

Building limestones/Spalling decay/Clay minerals swelling/Hydric dilation/Hygric dilation/X-ray diffraction/Transmission electron microscopy/Dilation Kinetic

1. Research aim:

Numerous studies evidence the drastic impact of the deformation recorded during water content variations (hydric dilation) on the spalling decay of building sandstones. Clay minerals able to swell when hydrated (swelling layers) are recognized as a key factor in this physical mechanism but no direct quantitative relationship is driven. In parallel, recent progresses made on the profile modeling procedure of experimental X-ray diffractograms allow accurate clay minerals quantification. Beneficiating from these advances, the present study aims at improving the understanding of the physical mechanism leading to spalling of bioclastic limestones. The investigations focus on the relationships between the spalling sensitivity, the swelling layers content and accessibility to water, the water transport properties, and the hydric dilation of limestones.

2. Introduction

Most of the medieval historical buildings of the Provence region (South East of France) were erected with a range of bioclastic limestones called “Pierre du Midi” deposited during the Miocene age (Burdigalian, 20−16 Ma). Deposition and diagenesis conditions have led to heterogeneous materials. Examining masonries of comparable exposure times reveals that some building stones are deeply affected by a spalling phenomenon while others remain well preserved despite of centuries of weathering. The church Saint Maurice of Caromb (Fig. 1) displays a good example of the different degrees of spalling.

The spalling decay [1] corresponds to the progressive loss of plates of stone surfaces exposed to rain and/or runoff whatever their position in the architecture. This decay pattern appears independently of any preferential orientation (bedding, lamination or stratification) and is clearly linked to some intrinsic properties of the stone material [2]. Numerous studies deal with this decay focusing on hydric dilation measurements [3, 4, 5, 6, 7, 8] combined to clay identification [4, 5] or semi-quantification [3, 6, 7]. Specific methods such as durability test [7], experimental warping test [8], and swelling pressure measurement [5, 8] are also invoked to understand this phenomenon. The

investigations mainly focus on sandstones and clay minerals are clearly identified as key factors in the spalling process.

Some of these minerals can experience intracrystalline swelling resulting from the hydration of the charge-compensating interlayer cations [9, 10]. They are called “swelling layers” and can be found as discrete clay minerals corresponding to the stacking of one layer type (smectite and/or vermiculite) as well as inside mixed layer minerals (MLM *e.g.* illite-smectite, chlorite-smectite, etc.) where they are stacked with one or more other layer types [11]. Some other factors related to the presence of clay minerals have been evoked such as the intercrystalline (osmotic) swelling [5] and their distribution within the texture [6]. The importance of these swelling mechanisms is widely recognized in civil engineering [12]. Apart from the impact of clay minerals, the roles of disjoining pressure, pore size distribution, structural anisotropy, mechanical strength and softening, thermal expansion of minerals, and hygric dilation are widely discussed [4, 5, 6, 7, 8]. The two mains hypotheses formulated in the literature imply the formation of shear stresses at the discontinuity between the wet outer layer and the dry inner core [8]. The first one suggests that it occurs during the wetting and is scaled by the compressive strength of the stone. The second one relates this mechanism to the beginning of the drying phase were the tensile strength of the stone is solicited. Nevertheless, the process responsible for fracture formation is not fully understood yet.

The severe spalling decay affecting historical building in the South East of France motivated a research work on the Miocene bioclastic limestones [13]. A new methodology was applied to identify the composition of clay minerals and to quantify accurately each of them. The results have shown that the sensitivity to spalling is related to their content in swelling layers within glauconite/montmorillonite mixed layer minerals. In the present paper, new investigations were conducted to go deeper in the understanding of the physical processes responsible for the spalling decay. Three types of “Pierre du Midi” with varying sensitivity to spalling were studied in terms of petrography, petrophysical properties, overall and clay mineralogy, and hydro-mechanical behavior. The obtained results were systematically compared to a reference type of “Pierre du Midi” considered unaffected by spalling. The present study thus aims at establishing the link between the swelling layers

content, localization, and the dilation behavior of stones under hydric and hygric conditions. In addition, the potential influence of water transfer properties and texture will be addressed.

3. Materials and methods

3.1 Origin of samples and sensitivity to spalling decay

Four types of "Pierre du Midi" were examined (Caromb grey: CARO-G, Caromb yellow: CARO-Y, Crillon: CRIL and Estaillades: ESTA) in this study. The medieval buildings erected with these types of limestones show a contrasting sensitivity to spalling decay [13]. CARO-G is highly sensitive; CARO-Y and CRIL show a moderate sensitivity as only few and thin plates are observed; and ESTA appears free from any spalling decay. This last sample was used as a reference material.

The considered samples from Caromb stone were taken from deposits of ancient building stones (CARO-G I and CARO-Y I) and from abandoned quarries formerly used to supply the building sites (CARO-G II and CARO-Y II, also studied in [13]). Crillon stone is increasingly used as replacement stone in buildings erected with the Caromb stone. Two samples (CRIL I and CRIL II, this last sample being also studied in [13]) were taken from one of the active quarries located in the village of Crillon-Le-Brave, a few kilometers from Caromb. Finally, the reference sample from Estaillades stone (ESTA) was taken from an active quarry near the village of Oppèdes in the same geographical area.

3.2 Methods

The petrographic description of the seven samples (CARO-G I, CARO-G II, CARO-Y I, CARO-Y II, CRIL I, CRIL II, and ESTA) was done using polarized light microscopy (Olympus BX-51) on thin sections.

Petrophysical properties (effective porosity, Hirschwald coefficient, and capillarity) of each of the seven samples were measured on six cores (h = 80 mm, d = 40 mm) drilled perpendicularly to the bedding plane according to the French and European standards (NF B10-503, EN 13755, and NF B10-

502). The pore size distribution was also examined for CARO-G II, CARO-Y II, CRIL II, and ESTA with mercury intrusion porosimetry (MIP) on ≈ 1 cm^3 specimens with a Micrometrics AutoPore IV porosimeter. The specific surface area (S_s) was estimated from MIP.

Mineralogical characterization was conducted by calcimetry (NF X 31-105) and X-ray diffraction (XRD) on total and acid (acetic acid 0.2 N) insoluble powders for the seven samples. Diffractograms were recorded on a Bruker D8 Focus diffractometer (Co K_α radiation) equipped with a Lynx'Eye detector operating with an aperture of 1 °2θ.

Clay mineral identification and quantification were done on the clay fraction (considered hereafter as <4μm) of all the samples through the combination of transmission electron microscopy (TEM, JEOL JEM 2011) coupled with an energy-dispersive X-ray spectrometer (EDX, X-Flash Silicon Drift Detector 5030, Bruker) and profile modeling of XRD patterns of oriented preparations. Details on the elemental quantification and structural formula calculation from TEM microanalysis can be found in [13]. XRD patterns were collected on oriented preparations saturated with calcium (Ca) at 0.01426 °2θ step intervals from 2.5 to 60 °2θ, using a 4 seconds counting time per step. A first set of XRD patterns was acquired after drying at room temperature (Ca + AD), then the same preparations were exposed to ethylene glycol (Ca + EG) vapor for at least 24 hours, and re-analyzed. All the experimental XRD patterns were fitted over the 4.5 – 60 °2θ CoKα range using the ASN program [14, 15, 16]. The fit quality was estimated using the unweighted profile Rp-factor [13].

The deformation (ε) experienced by the stone samples resulting from water content variation was evidenced by dynamic follow up of one dimension through time (72 hours) for all the samples. The measurements were systematically carried out perpendicularly to the bedding planes (maximum dilation). Displacements were recorded inside a climatic chamber at a constant temperature of 23.0 + 0.1 °C on 6 core samples per limestone type in both hygric (relative humidity change from 30 to 95%) and hydric (immersion in 2 centimeters of water) conditions by LVDT sensors (Solartron ® LE/12S, resolution of 0.2 μm). Finally, uniaxial compressive strengths were measured for CARO-G I, CARO-Y I, CRIL I, and ESTA on both dry and water saturated cores (6 cores per samples, NF EN 14580).

4. Experimental results

4.1 Petrographic description

The investigated limestones belonged to the bioclastic packstones (Dunham) class. Their texture was characterized by the presence of bioclastic fragments (Red Algae, Bryozoans, Bivalvia, Echinoderms, Forams, and lithoclasts) and two groups were distinguished (Fig. 2). Large fragments (> 500 μm) cemented by a sparse and unevenly distributed calcareous matrix were observed in CARO-Y, CRIL, and ESTA. Fragments of smaller dimensions (< 200 μm) dispersed in a greyish marl matrix were recognized in CARO-G together with ferruginous coatings (also in CARO-Y) and glauconite grains. Angular quartz grains (~ 200 μm) as well as greenish glauconitic fillings of bioclasts (mainly Bryozoans) were present in all samples except ESTA (Fig. 2).

4.2 Main petrophysical properties

The limestones sensitive to spalling displayed an effective porosity ranging from 15.0 (CARO-G II) to 23.2% (CRIL II) (Table 1). The ratio of the porous volume accessible to water under atmospheric conditions over the porosity accessible to water under vacuum (Hirschwald coefficient, *S*) varied between 0.62 (CRIL II) and 0.94 (CARO-G II). For most of the samples, around 30% of the porous volume remained free of water during water imbibition in environmental conditions ($S \sim 0.70$) whereas almost all (0.94) of the pore space of CARO-G II was invaded in the same conditions.

The pore size distribution of CARO-G II and CRIL II was unimodal. Their mean pore radii differed however greatly (Table 1). CRIL II was mainly macroporous (R_a = 7.6 μm) whereas CARO-G II was microporous (R_a = 0.1 μm). CARO-Y II displayed a wider and bimodal pore size distribution (meso and macropores). The very high water saturation level (*S*) measured for CARO-G II could be linked to its microporous capillary medium and an assumed good connectivity between the pores. The specific surface area (surface allowing physico-chemical exchanges) varied from 1.43 (CRIL II) to 9.52 $m^2\ g^{-1}$ (CARO-G II), proportionally to the microporosity.

Capillarity was approximatively proportional to porosity in these limestones and the results ranged from 0.18 (CARO-Y I) to 0.36 (CRIL II) g cm^{-2} $h^{-1/2}$ for the capillary coefficient, and from 1.3 (CARO-Y I) to 2.9 (CRIL II) cm $h^{-1/2}$ for the velocity of capillary rise (Table 1). Note that a high standard deviation was calculated for CARO-G II.

Compared to the other samples (Table 1), the reference sample ESTA displayed a high total porosity (N = 31.7%), a relatively high Hirschwald coefficient (S = 0.79), a wide pore size distribution with a perfect bimodal distribution, high capillarity coefficients (A = 1.75 g cm^{-2} $h^{-1/2}$ and B = 7.4 cm $h^{-1/2}$), and a low specific surface area (S_s = 0.76 m^2 g^{-1}).

4.3 Overall mineralogy

The relative proportions of carbonates, quartz and feldspar, and clay fraction of each sample deduced from calcimetry, XRD on total and acid insoluble powder, and clay fraction separation were presented in a ternary diagram (Fig. 3). The insoluble fractions varied from 0 (ESTA) up to 30% (CARO-G II). Various proportions of detrital or authigenic inputs (quartz, feldspar, hematite, rutile, goethite, and clay minerals) and insoluble carbonates (ankerite and siderite) were identified. In comparison, ESTA was considered as a pure limestone (100% calcite, as evidenced by powder XRD and calcimetry tests) in agreement with the petrographic observations (Fig. 2). Thus, neither clay minerals separation nor quantification was made for this sample.

The abundance of the clay fraction (< 4 μm) of the rest of the studied limestones varied from 1.2 (CRIL I) to 9.8% (CARO-G II) (Fig. 5). The clay minerals composing the clay fractions must be localized in the glauconitic grains (CARO-G) and the glauconitic fillings (CARO-Y, CRIL) observed inside the tests of the bioclasts (Fig. 2). Note that the greyish marl matrix of CARO-G was also composed by a large amount of clay-sized materials explaining the relative abundance of its clay fraction (9.8%).

4.4 Clay minerals quantification

The experimental XRD patterns acquired on oriented mounts of the clay fractions (Fig. 4) displayed few *hkℓ* reflections of accessory minerals (quartz: 0.426 nm and 0.334 nm; K and/or Na feldspar: 0.325 nm and 0.320 nm; siderite: 0.279 nm) in all samples.

The combination of XRD and TEM-EDX results allowed identifying five different clay mineral phases (three discrete phases: muscovite, glauconite, and sudoïte; and two mixed-layer minerals or MLMs: glauconite/montmorillonite and glauconite/sudoïte) composed by four different clay mineral layers. The mean structural formulas of the discrete phases were calculated for each sample from the TEM-EDX results (see [13] for details on crystal chemical composition of each phase). The deficient mica chemical composition was attributed to glauconite in agreement with the petrographic observations (Fig. 2). For MLM composed by glauconite and montmorillonite (swelling layers), a theoretical structural formula of a Fe-rich montmorillonite ($Si_4O_{10}(Fe_{1.6}Mg_{0.4})OH_2Ca_{0.2}$) with various water molecule content (0, 1, or 2 H_2O per unit cell) was hypothesized whereas that of the glauconite end-member was set as the equivalent discrete phase. For the other MLM, both glauconite and sudoïte were computed with structural formulas of the equivalent discrete phases.

The structural formulas were used as constraints for the profile modeling of the experimental diffractograms acquired in AD and EG state (see example of CARO-G I in Fig.4). The contributions of each phase to the calculated intensity were presented with regard to the experimental pattern. All samples displayed the diffraction dome occurring at ~ 1.45 nm in the AD state (Fig. 4a) and shifted toward lower angles (~ 1.725 nm) in the EG state (Fig. 4b). This feature illustrated the presence of the glauconite/montmorillonite MLM containing a significant amount of swelling layers. The relative proportions of each phase in the calculated pattern were given in the pie charts. Ultimately, the total content of each clay minerals layer was calculated from (i) the composition of the different MLMs and discrete phases, (ii) the relative proportion of each phase in the clay fraction, and (iii) the relative proportion of the clay fraction in the sample (Fig. 5). The results highlighted the predominance of

mica-like layers (muscovite and glauconite) in all samples. The swelling layer (montmorillonite, Fig. 5) content varied from 0.3 (CRIL I) to 1.3% (CARO-G II).

4.5 Hydromechanical behavior

The dynamic follow up of one dimension of the core samples through time allowed determining the hygric and hydric dilation coefficients. A large difference between these two coefficients was systematically measured and the hydric dilation coefficient is more than twice the hygric dilation one. The results of these two sets of experiments were summarized (Table 1) by the mean values (ε_{hyg} and ε_{hyd}). Hygric dilation coefficients (CARO-G I, CARO-Y I, and CRIL I) ranged from 0.022 to 0.122 mm m^{-1}. A maximum value of 0.171 mm m^{-1} was measured on CARO-G I. Hydric dilation coefficients were distributed from 0.041 (CARO-Y I) to 0.722 mm m^{-1} (CARO-G II) with a maximum value of 1.015 mm m^{-1} measured on CARO-G II. Barely any variations (ε_{hyd} = 0.014 $\pm$ 0.008) in dimension were measured on the reference sample (ESTA).

Finally, the uniaxial compressive strengths measured on core samples dry (R_{dry}) and saturated with water (R_{sat}) showed a wide range of values (Table 1). As expected the uniaxial compressive strength of the most porous material (ESTA) was the lowest measured (R_{dry} = 10.5 MPa) in comparison with the other types displaying close and higher values. The studied limestones were ranked as moderately resistant (R < 30 MPa) according to conventional classification of building limestones. The percentage of mechanical strength loss induced by water saturation (softening) varied from 29.9% (CRIL I), 52.4% (ESTA), and up to 59.6% in the case of CARO-G I.

5. Discussion

Previous research works dealing with spalling of building sandstones points out the preeminent impact of the hydric dilation behavior and swelling clay minerals [3, 4, 5, 7, 8]. In the present study, the Estaillades stone, selected as a reference material insensitive to spalling, has a very low hydric dilation and no clay minerals. On the opposite, all the samples of bioclastic limestones

sensitive to spalling (Caromb and Crillon stones) exhibited significant hydric dilation and MLM containing swelling layers. These two parameters are thus clearly involved in the spalling process of limestones in the same way than in sandstones.

5.1 Identification and origin of the swelling layers

The clay fraction of the studied limestones remained low in absolute percentage (< 10%). The combination of XRD and TEM-EDX allowed identifying swelling layers within this clay fraction however dominated by non-swelling mica (muscovite) and deficient mica (glauconite) layers. The swelling layers were systematically montmorillonite layers interstratified with glauconite layers inside a MLM phase. They must be located in the glauconite grains or greenish glauconitic fillings of bioclasts as these clay minerals associations [9] are known to show considerable mineralogical variability evolving through maturation from smectite-like phases to pure glauconite (glauconitization process) within sedimentary deposits [17].

5.2 Influence of swelling layer content on the hydric dilation

Hydric dilation of 2.9 mm m^{-1} is measured in Tarifa brown sandstones [8] containing 7% of clay minerals but neither the proportion of smectite/chlorite mixed layers minerals nor of swelling layers (smectite) are determined. The relationship between hydric dilation (from 0.28 to 0.94 mm m^{-1}) and smectite contents (from 1.1 to 6.8%) of Macigno sandstones [3] shows a positive correlation (R=0.70) but the smectite content was only estimated through decomposition of X-ray diffractograms. Here, the methodology of clay mineral quantification based on the combination of TEM-EDX structural formula calculation and XRD profile modeling [13] offered a valid and reproducible way to calculate the mass proportion of swelling layers. The results varied from 0.0 (ESTA) to 1.3% (CARO-G II) (Fig. 5) and as expected, these growing proportions were clearly linked to the specific surface areas. The corresponding hydric dilations ranged between 0.04 and 0.72 mm m^{-1} and were comparable to those acquired on Macigno sandstones [3] in amplitude. The amount of swelling layers quantified for the “Pierre du Midi” limestones was however much lower than the one estimated for the Macigno

sandstones. Note that the studied limestones were also much more porous and brittle than the Macigno sandstones [3].

The relationship between the absolute quantities of swelling layers and the hydric dilation coefficients was plotted (Fig. 6) and fitted by a positive linear relationship satisfactory (R^2 = 0.85). This relationship highlighted that the higher the swelling layers content, the higher the hydric dilation coefficient. Nevertheless, the strength of this relationship was reduced by the relatively low hydric dilation of CARO-Y I, CARO-Y II, and CRIL II with regard to their swelling layers content. Other parameters that will be addressed later in this discussion (5.4) may play a part in the reduction of the swelling amplitude. Note that as already highlighted for sandstones [5], the hygric dilation was significantly lower than the hydric one.

5.3 Relation between swelling layers, hydric dilation, and sensitivity to spalling

The classification of the studied limestones in three classes of sensitivity to spalling appeared well correlated to their swelling layers content and hydric dilation (Fig. 6). The expansive nature of smectite (montmorillonite) mixed-layer minerals causes them to be extremely reactive in environments with changing environmental conditions [9]. The intracrystalline swelling of these layers could be interpreted as a triggering factor for the hydro-mechanical behavior. At the microscopic scale, the invasion of the porous network by water molecules provokes the swelling of the interlayer space of the swelling layers driving the displacement of the surrounding mineral grains. These displacements can be partially accommodated by the porous volume but a part may be transmitted to the solid matrix and result in hydric dilation. Few authors attempted to measure the swelling pressure developed by this phenomenon with experimental devices [5, 8]. The obtained values (0.03 to 0.84 MPa) are however much lower than those expected from calculation. They are also lower than the tensile strength of the studied stones by at least one order of magnitude. This could be due to stress relaxation of the wet material caused by softening associated with delayed clay swelling. Further studies on swelling pressure and mechanical damage driven by hydric dilation need to be carried out to understand the mechanism accounting for the formation of plates in the spalling decay.

5.4 Possible impact of water transfer properties and texture

On the opposite to what other authors found regarding sandstones [3, 5, 8], no relationship was evidenced between hydric dilation and pore size distribution. Indeed, the importance of the microporosity was in accordance with the absolute proportion of clay minerals (Table 1and Fig. 5). This could be explained by the fact that clay minerals display a finely divided structure organized in aggregates delimited by micropores [9].

The hydric dilation experiments were conducted in the same conditions than the capillarity test, thus the evolution of water intake through time was compared to the consecutive hydric dilation (Fig. 7). In all capillary curves, the transition between the two phases corresponds to the end of the capillary imbibition, *i.e.* when the water reaches the top of the core. Regarding these two experiments and their coupling, two different behaviors were observed. CARO-G I and CARO-G II displayed a fast hydric dilation that stabilizes after ~ 20 hours. This evolution followed almost perfectly the water intake suggesting a homogeneous distribution and a good accessibility of reactive mineral surfaces in the texture. This is in agreement with their higher clay fraction and the presence of a clay sized matrix (marl matrix) between the grains (Fig. 2) constituting a well-connected porous network (high Hirchwald coefficients, Table 1). On the contrary, CARO-Y I, CARO-Y II, CRIL I, and CRIL II had a more linear hydric dilation and no plateau was observed after 72 hours (Fig.7). The maximal hydric dilation of these samples was not reached at the end of the experiment. These materials displayed a net delay of the hydric dilation process with respect to the water uptake. This specific kinetic of dilation gave a good explanation to the relatively low hydric dilation of CARO-Y I, CARO-Y II, and CRIL II with respect to their swelling layers content. This combination could contribute to their moderate sensitivity to spalling (Fig.6) meaning that some of the reactive mineral surfaces triggering the dilation remain dry during water intake. The fact that the swelling layers are mainly located inside glauconitic fillings of bioclasts in these samples (Fig. 2) supports this argument. Therefore, in addition to their absolute content, the textural distribution of swelling layers has a great impact on the dilation kinetic.

As it was free from any clay minerals, the reference material (Estaillades limestone) offered the possibility to describe the role of water transfer in the dilation behavior. The dilation curve (Fig. 7) reached a plateau exactly when the capillary curve showed its transition. The hydric dilation measured is thus clearly driven by the capillary intake. This could be interpreted as the role played by the disjoining pressure produced in the micropores (<0.1μm) during water imbibition (see, for instance, discussion in [5]).

5.5 Mechanical strength and softening

Eventually, some results showed that water saturation provokes a drastic reduction of the mechanical strength of limestones (Table 1) as already pointed out in the literature [18]. This softening is also reported for sandstones [2] and is attributed to both inter- (osmotic) and intra-crystalline swelling of clay minerals in Tarifa sandstones [7] and to hydric dilation in various German sandstones [5]. Here, the softening affected all the bioclastic limestones studied, with and without any clay minerals, but to a variable extent. The deduced degree of softening was not correlated to hydric dilation. Note that other mechanisms such as reduction of the bonding energy among grains and stress corrosion phenomena [19] were also proposed. This lowering of the mechanical properties [8] certainly plays a role in the fracturing of the wetted stone surface occurring during the spalling process.

6. Conclusions

Six bioclastic limestones of contrasting sensitivity to spalling were compared to a reference material of the same geological formation and unaffected by this decay mechanism. Based on usual classifications, the reference material could be regarded as the less durable (higher porosity, higher capillarity, lower mechanical strength) but the lack of any clay minerals preserves it against spalling. Limestone types considered more durable suffer from this specific decay in an extent that can be evaluated only by the swelling layers content. These were identified as glauconite/montmorillonite mixed layers minerals. Their absolute content can be considered low (< 1.3%) with respect to the

whole fraction but the results underlined their decisive influence on the macroscopic physical process of hydric dilation and its amplitude. Their localization in the texture has also a strong impact on the hydric dilation kinetics. Therefore, the dilation behavior of limestone, known as decisive in the spalling mechanism, appears to be triggered by these reactive mineral surfaces. This swelling mechanism can also lead to mechanical stresses that may cause the fracture of stone exposed surfaces. Thus, the swelling layers content should be considered in the definition of durability in order to predict spalling sensitivity.

Further interpretation of results highlighted that swelling layers content and localization are not the only factor involved in this decay mechanism. The mechanical softening experienced by the stones during variations of water content could also enhance spalling. A perspective of the research project including the present paper aims at further understanding the origin of this process.

Acknowledgments

The authors would like to thank the French Ministry of Culture and Communication for financing this study in the frame of a national research program for the knowledge and conservation of cultural heritage materials (PNRCC), Vincent Mercurio (CICRP) for thin section preparation, and Odile Guillon (CICRP) for providing the pictures used in figure 1.

References

[1] V. Vergès-Belmin (ed.), Illustrated glossary on stone deterioration patterns, ICOMOS International Scientific Committee for Monuments and Sites, 2008.

[2] J. Delgado Rodrigues, Evaluacion del comportamiento expensive de las rocas y su interés en conservacion, Materiales de Construcción 51 (2001) 183–195.

[3] M. Franzini, L. Leoni, M. Lezzerini, R. Cardelli, Relationships between mineralogical composition, water absorption and hydric dilatation in the « Macigno » sandstones from Lunigiana (Massa, Tuscany), European Journal of Mineralogy 19 (2007) 113–123.

[4] E. Sebastian, G. Cultrone, D. Benavente, L.L. Fernandez, K. Elert, C. Rodriguez-Navarro, Swelling damage in clay-rich sandstones used in the church of San Mateo in Tarifa (Spain), Journal of Cultural Heritage 9 (2008) 66–76.

[5] J. Ruedrich, T. Bartelsen, R. Dohrmann, S. Siegesmund, Moisture expansion as a deterioration factor for sandstone used in buildings, Environmental Earth Science 63 No. 7-8 (2011) 1545–1564.

[6] E. Colas, J-D. Mertz, C. Thomachot-Schneider, V. Barbin, F. Rassineux, Influence of the clay coating properties on the dilation behavior of sandstones, Applied Clay Science 52 (2011) 245–252.

[7] D. Benavente, G. Cultrone, M. Gomez-Heras, The combined influence of mineralogical, hygric and thermal properties on the durability of porous building stones, European Journal of Mineralogy 20 (2008) 673−685.

[8] I. Jimenez-Gonzalez, C. Rodriguez-Navarro, G.W. Scherer, Role of the clay minerals in the physicomechanical deterioration of sandstone, Journal of Geophysical Research 113 F02021 (2008).

[9] A. Meunier, Argiles, GB Science Publisher, Paris, 2002.

[10] D.M. Moore, R.C.Jr. Reynolds, X-Ray Diffraction and the Identification and Analysis of Clay Minerals, Oxford University Press, 1997.

[11] S. Fiore, J. Cuadros, F.J. Huertas (ed.), Interstratified clay minerals: origin, characterization and geochemical significance, AIPEA Educational Series, Pub. No. 1 Digilabs, Bari, Italy, 2010.

[12] F.T. Madsen, M. Müller-Vonmoos, The swelling behavior of clays, Applied Clay Science 4 (1989) 143–156.

[13] J. Berthonneau, O. Grauby, E. Ferrage, J-M. Vallet, P. Bromblet, D. Dessandier, D. Chaudanson, A. Baronnet, Impact of swelling clays on the spalling decay of building limestones: Insights from X-ray diffraction profile modeling, European Journal of Mineralogy 26 (2014) 643−656.

[14] V.A. Drits, C. Tchoubar, X-ray diffraction by disordered lamellar structures: theory and applications to microdivised silicates and carbons, Springer-Verlag, Berlin, 1990.

[15] B. Lanson, B.A. Sakharov, F. Claret, V.A. Drits, Diagenetic smectite-to-illite transition in clay-rich sediments: a reappraisal of X-ray diffraction results using the multi-specimen method, American Journal of Science 309 (2009) 476−516.

[16] E. Ferrage, O. Vidal, R. Mosser-Ruck, M. Cathelineau, J. Cuadros, A reinvestigation of smectite illitization in experimental hydrothermal conditions: Results from X-ray diffraction and transmission electron microscopy, American Mineralogist 96 (2011) 207–223.

[17] A. Meunier, A. El Albani, The glauconite− Fe-illite− Fe-smectite problem: a critical review, Terra Nova 19 (2006) 95−104.

[18] B. Vásárhelyi and P., Ván, Influence of water content on the strength of rock, Engineering Geology 84 (2006) 70−74.

[19] W.C., Kowalski, L'influence des variations de teneur en eau sur la résistance mécanique et la déformation des roches dans la zone d'altération, Bulletin de l'Association Internationale de Géologie de l'Ingénieur 12 (1975) 37−43.

Sample	CARO-G I	CARO-G II	CARO-Y I	CARO-Y II	CRIL I	CRIL II	ESTA
Effective porosity N (%)	20.7 ± 0.5	15.0 ± 1.9	22.3 ± 0.2	19.8 ± 0.9	21.5 ± 0.2	23.2 ± 1.6	31.7 ± 0.7
Hirschwald coefficient S	0.72	0.94	0.68	0.64	0.63	0.62	0.79
Average pore radius R_a (µm)	-	0.1	-	0.2	-	7.6	1.3
Surface area S_s ($m^2.g^{-1}$)	-	9.52	-	2.35	-	1.43	0.76
Microporosity (%)	-	13.5	-	4.4	-	2.5	0.9
Mesoporosity (%)	-	2.8	-	11.5	-	4.5	15.9
Macroporosity (%)	-	2.3	-	7.3	-	14.5	10.6
Absorption coefficient A ($g.cm^{-2}.h^{-1/2}$)	0.19 ± 0.02	0.23 ± 0.26	0.18 ± 0.03	0.21 ± 0.02	0.28 ± 0.04	0.36 ± 0.11	1.75 ± 0.30
Capillarity fringe speed B ($cm.h^{-1/2}$)	1.4 ± 0.1	2.2 ± 0.2	1.3 ± 0.2	2.0 ± 1.0	2.7 ± 0.2	2.9 ± 0.7	7.4 ± 0.1
Compressive strenght R_{dry} (MPa)	17.8 ± 5.1	-	24.5 ± 3.2	-	24.4 ± 2.6	-	10.5 ± 0.5
Compressive strenght R_{sat} (MPa)	7.2 ± 2.2	-	14.3 ± 2.3	-	17.1 ± 2.1	-	5.0 ± 1.5
Softening (%)	59.6	-	41.6	-	29.9	-	52.4
Hygric dilation ε_{hyg} ($mm.m^{-1}$)	0.122 ± 0.037	-	0.022 ± 0.003	-	0.040 ± 0.008	-	-
Hydric dilation ε_{hyd} ($mm.m^{-1}$)	0.337 ± 0.093	0.722 ± 0.325	0.041 ± 0.030	0.070 ± 0.022	0.157 ± 0.105	0.104 ± 0.051	0.014 ± 0.008

Table 1. Main petrophysical properties of the bulk samples measured perpendicularly to the bending plane. The different class of porosity correspond to the volume fraction (%) of pores with radius $r <$ 0.1 µm (micro), $0.1 < r < 5$µm (meso), and $r > 5$µm (macro).

Figure 1. Views of church Saint Maurice of Caromb (14th century, Vaucluse, France) showing the high degree of spalling decay on the bell tower (A), and the eastern façade (B). The superficial state allows distinguishing a limestone type strongly affected by spalling (grey facies) from one moderately affected (yellow facies). Details highlight the progressive plate formation affecting a grey ashlar viewed from the side (C): the plates vary in thickness and are isolated from the bulk by a fractured zone.

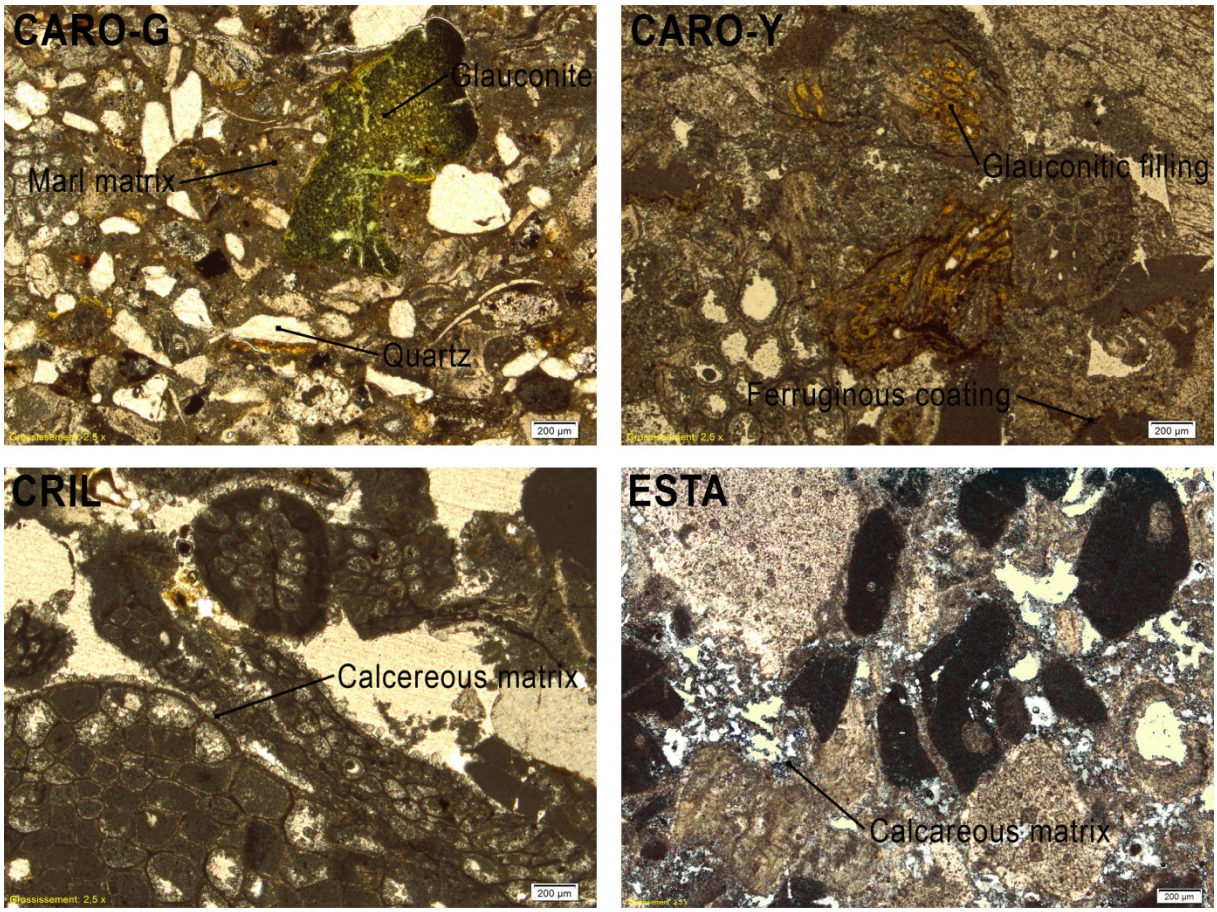

Figure 2. Microphotographs of samples CARO-G, CARO-Y, CRIL, and ESTA acquired in polarized light microscopy.

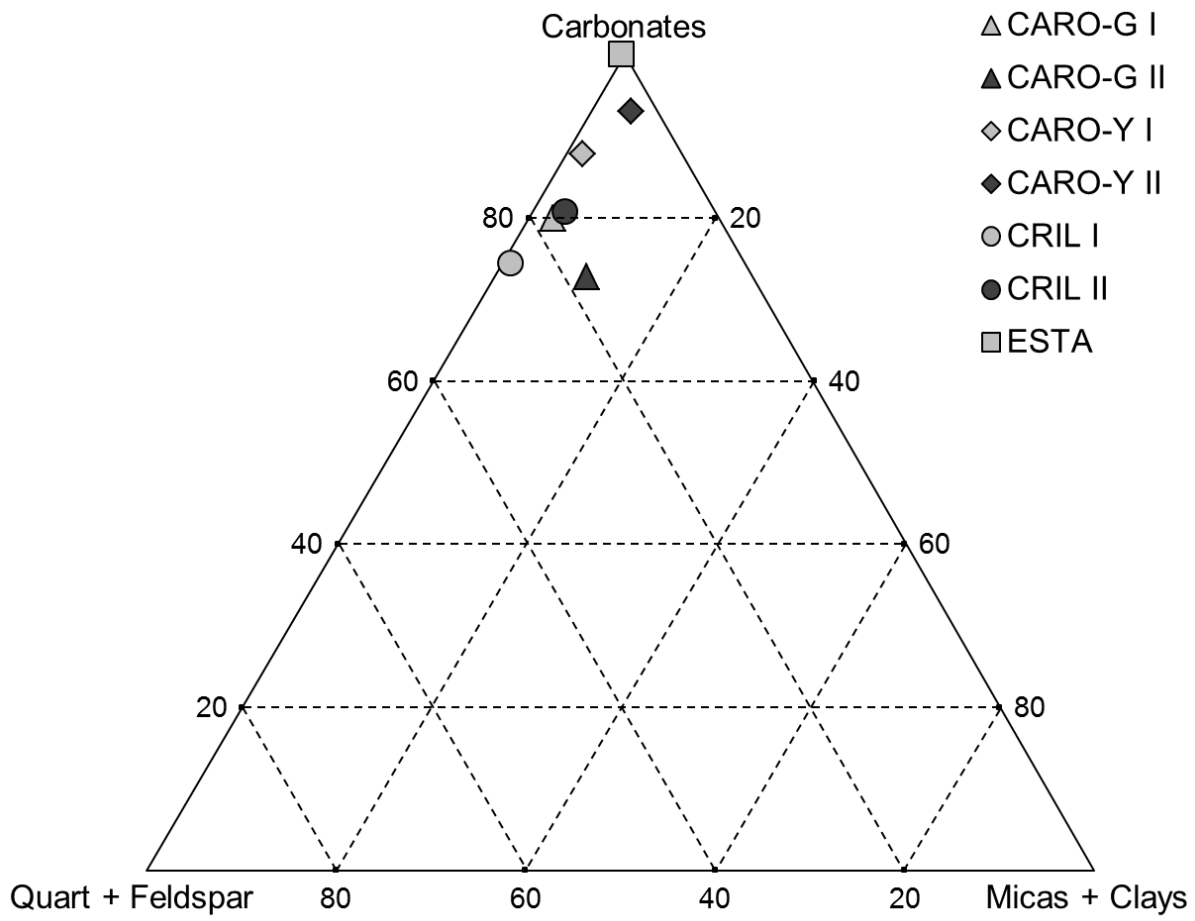

Figure 3. Ternary diagram displaying the contents of carbonates, quartz and feldspar, and micas + clay minerals of the studied limestone samples.

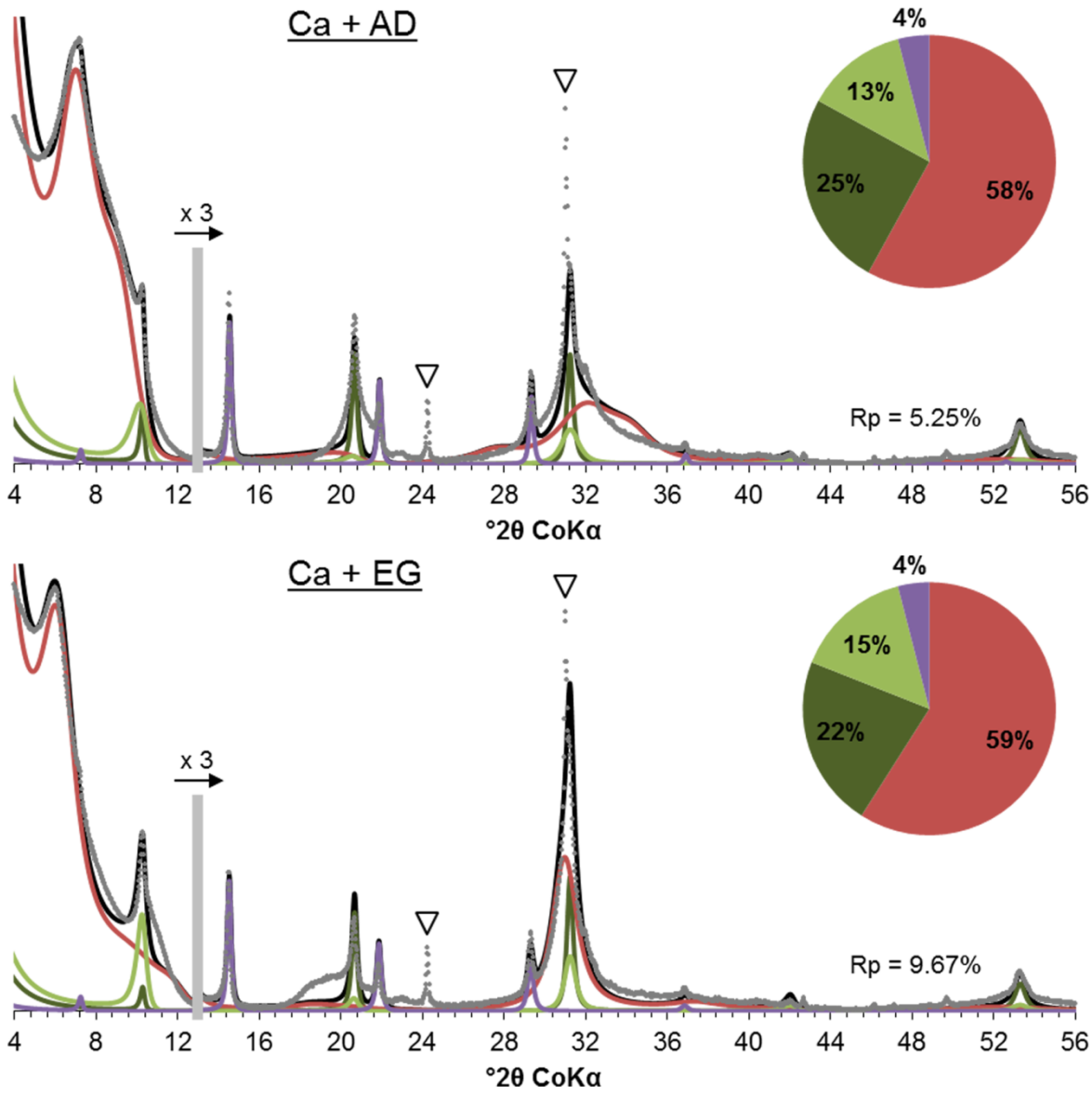

Figure 4. Experimental (crosses) and modeled (solid black lines) XRD profiles of samples CARO-G I air dried (Ca + AD, top) and saturated with ethylene glycol (Ca + EG, bottom). The respective contributions of the various phases to the calculated XRD profiles are shown in light red (MLM glauconite/montmorillonite), light green (glauconite), green (muscovite), and purple (sudoïte). The pie charts present the relative proportions of these phases whereas open triangles indicate the presence of additional quartz reflections. The grey bar topped by the label "x3" means that for diffraction angles greater than 13°2θ, the diffracted intensities (measured and calculated) were multiplied by 3.

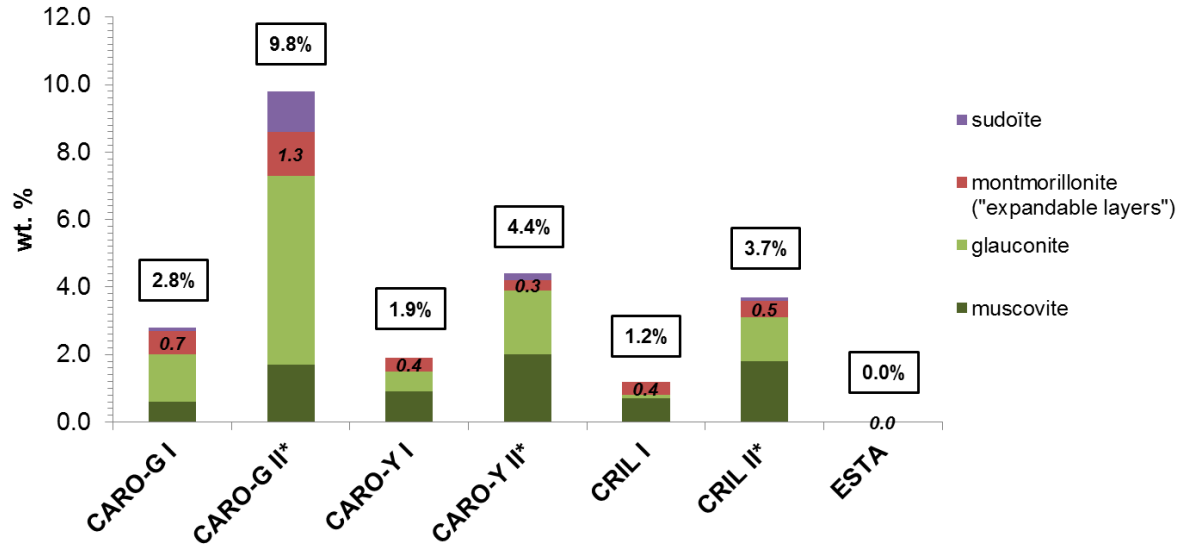

Figure 5. Results of the clay mineral layers quantification from the profile modeling of experimental X-ray diffractograms Ca + EG. Total clay contents are given in the framed boxes above the graphs and the absolute swelling layers contents are labelled in the corresponding bars. *clay mineral quantification results from [13].

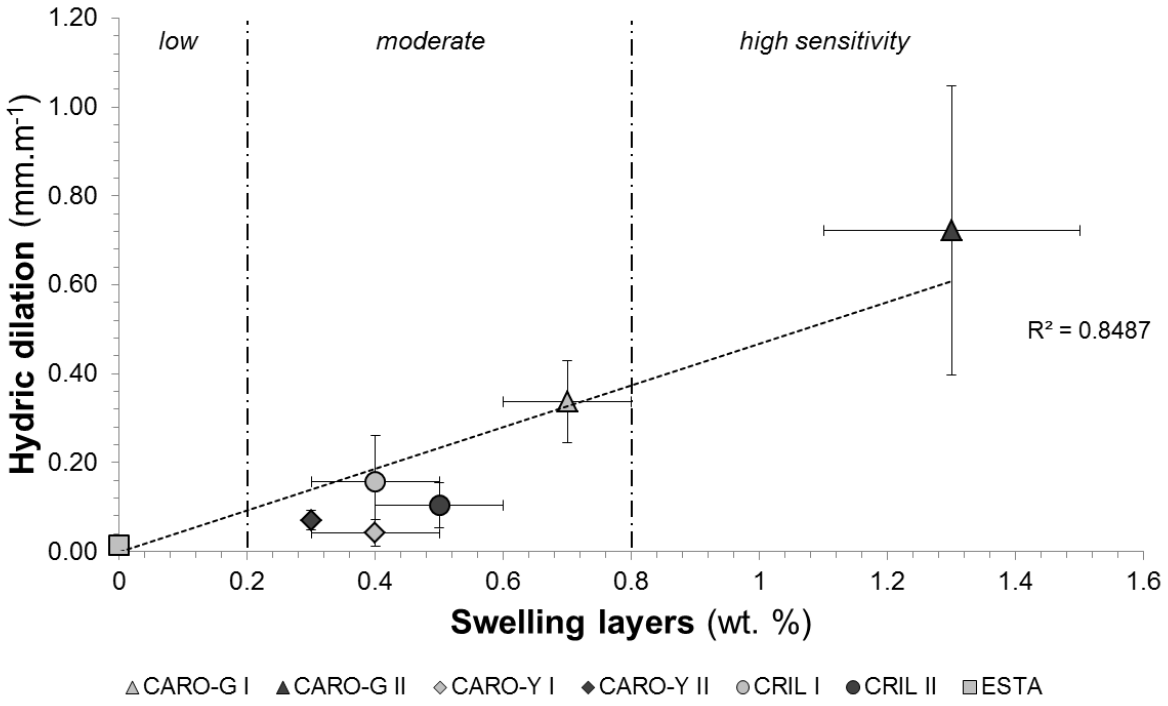

Figure 6. Mean hydric dilatation coefficients of the seven studied samples as a function of their amounts of swelling layers. The limits between low, moderate, and high sensitivity to spalling decay were placed according to [13].

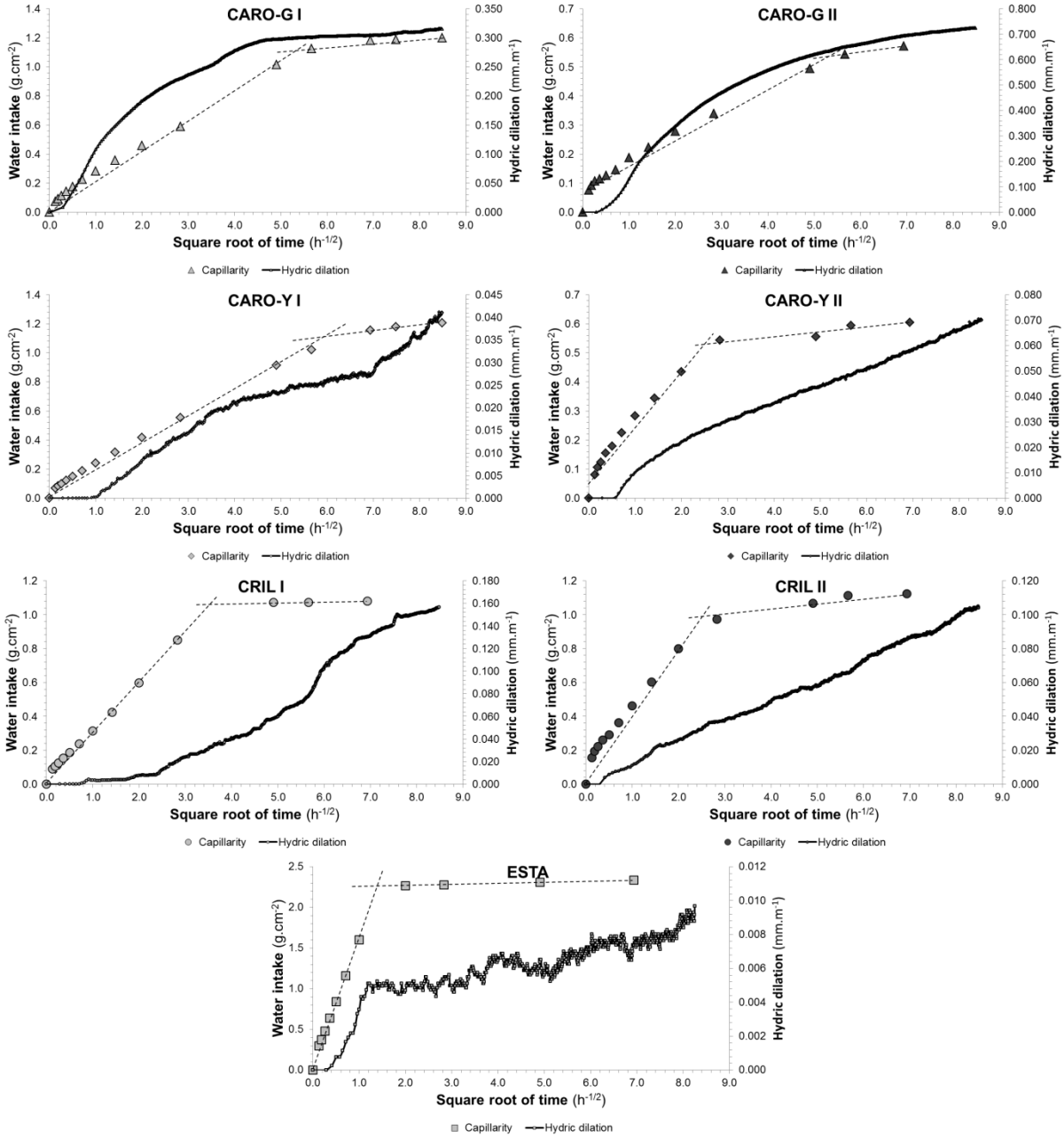

Figure 7. Evolution of the mean hydric dilation and water intake (capillarity test) with respect to the square root of time.